ACS Photonics

pubs.acs.org/journal/apchd5

Letter

Nonlinear Optical Absorption of ReS_2 Driven by Stacking Order

Yongjian Zhou, Nikhilesh Maity, Jung-Fu Lin, Abhishek K. Singh, and Yaguo Wang*

Cite This: *ACS Photonics* 2021, 8, 405–411

Read Online

ACCESS | Metrics & More | Article Recommendations | Supporting Information

ABSTRACT: The stacking order of 2D materials can result in fascinating physical properties. Two different stacking orders (AA and AB) were recently identified in ReS_2, a rising star in the transition metal dichalcogenides family with a unique anisotropic property. Their optical and vibrational properties show drastically different features. With intensity-scan spectrometry, the nonlinear optical absorption of both AA and AB stackings in ReS_2 was investigated. Saturable absorption (SA) only occurs in AB stacking at certain polarization angles, whereas it is absent in AA stacking. This saturation behavior is attributed to strong exciton−exciton annihilation (EEA). Excited-state absorption (ESA) is prominent in both stacking orders, but more anisotropic with polarization in AB stacking. Our results provide new insights in using ReS_2 as a nonlinear optical material in forefront optoelectronics.

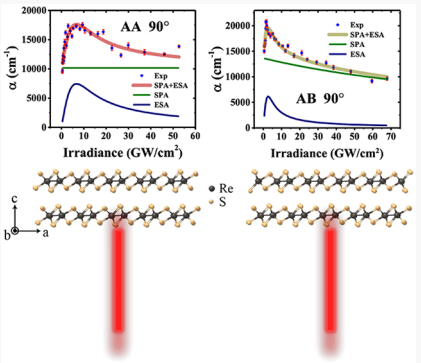

KEYWORDS: *stacking orders, rhenium disulfide, nonlinear absorption, first-principles calculations*

Layer alignment in 2D materials inherently gives different atomic stacking orders where many intriguing phenomena are observed. For example, in 2018, superconductivity was achieved in bilayer graphene at a certain "magic angle".[1] In 2019, Moiré excitons were realized in $MoSe_2/WSe_2$ heterostructures at small twisted angles.[2,3] Stacking order was also found to be important in manipulating nonlinear properties, such as inducing second order processes. In trilayer graphene with ABA stacking, where the centrosymmetry in the monolayer is broken, a second order susceptibility of around 0.9×10^{-10} m/V was observed with an excitation wavelength of 1300 nm,[4] while in ABC stacking, second order phenomena were not observed because centrosymmetry is still preserved. In MoS_2, a second harmonic generation was observed in the 3R phase regardless of the layer number, but in the 2H phase it is only seen with samples with an odd number of layers.[5] Very few studies have been devoted to the impact of the stacking order on nonlinear absorption for which 2D semiconductors have found many potential applications in optoelectronic devices.

ReS_2 is a rising star in the transition metal dichalcogenide family. The uniqueness of ReS_2 lies in its distorted 1T triclinic crystal structure where the additional *d* valence electrons of Re atoms form zigzag Re chains parallel to the *b*-axis, drastically reducing its symmetry. As a result, ReS_2 possesses extremely weak interlayer bonding and anisotropic optical,[6−8] thermal,[9] and electronic properties.[10,11] Unlike black phosphorus, ReS_2 is very stable in air, making it more suitable for optoelectronic applications. Recently, two stacking orders were identified in multilayer ReS_2:[12] AA stacking where adjacent layers sit right on top of one another with minimal displacement and AB stacking where adjacent layers shift by one-unit cell along the *a*-axis. The carrier dynamics and both optical and vibrational properties in different stacking orders were found to be drastically distinct. A few studies suggest that ReS_2 should be a promising candidate as a nonlinear optical material for lasers.[8,13] However, the impact of the stacking order on nonlinear optical properties in ReS_2 is unknown. In this work, we study the nonlinear absorption of ReS_2 of both AA and AB stackings with a home-built intensity scan (I-scan) spectrometer. It was found that both single-photon absorption (SPA) and ESA are more anisotropic in AB stacking. The saturation irradiance associated with the SPA is only prominent in AB stacking (negligible in AA stacking) at polarization angles from 30° to 105°, which is attributed to strong EEA along those polarizations. Orbital resolved band structures calculated with first-principles simulation suggested that the probability of the optical transition of Exc. III could be much higher in AB stacking than AA stacking. Our results reveal that stacking order is a critical factor when considering ReS_2 as a nonlinear absorption material for optoelectrical applications.

The samples were exfoliated from a bulk crystal (HQ graphene). Stacking orders can be identified using optical Raman spectra measured in a Raman spectroscopy, as shown in Figure 1a,d.[12,14] The displacement between Mode III and Mode I is roughly 20 and 13 cm^{-1} for AB and AA stacked

Received: August 3, 2020
Published: January 29, 2021

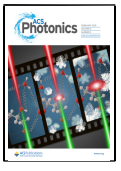

https://dx.doi.org/10.1021/acsphotonics.0c01225
ACS Photonics 2021, 8, 405−411

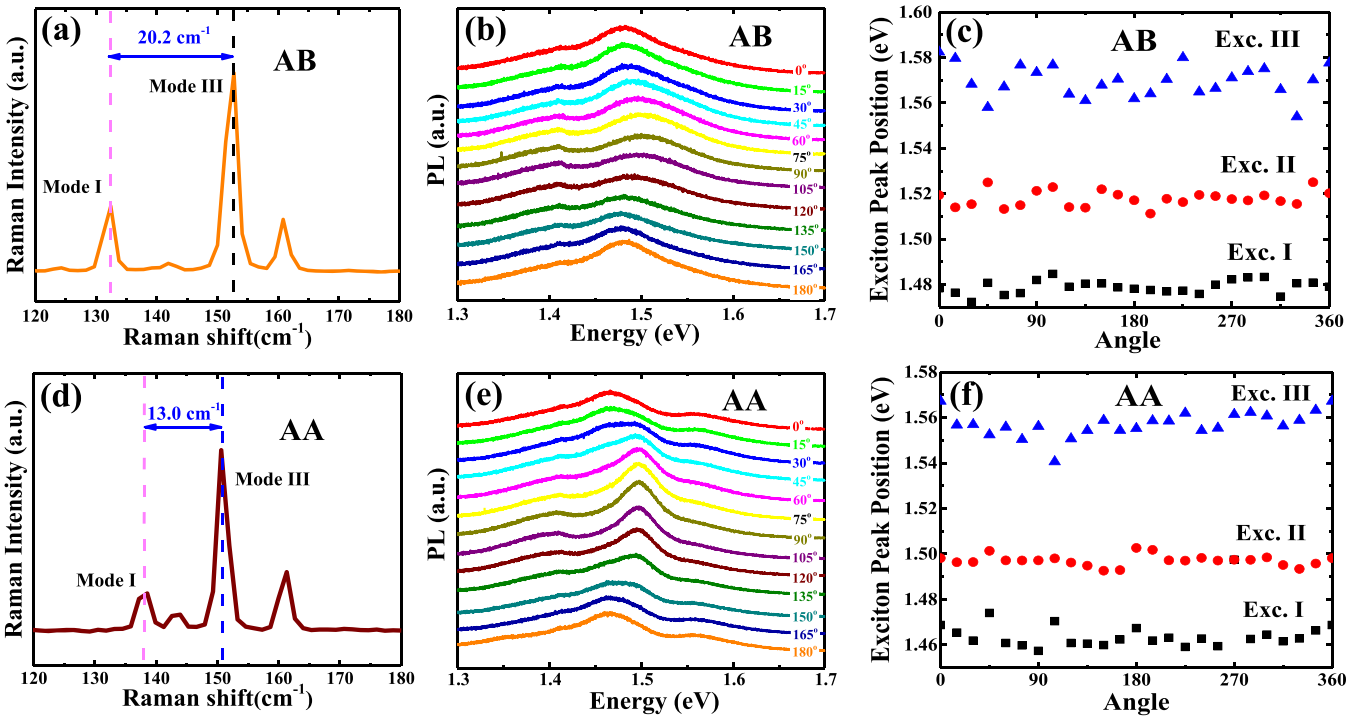

Figure 1. Different stacking orders characterized by Raman and PL. (a, d) Raman spectra of AB and AA stacking, respectively. (b, e) PL spectra for stacking AB and stacking AA, as a function of polarization angle of collection beam, respectively. (c, f) PL peaks of Exc. I, II, and III for stacking AB and AA as a function of the polarization angle of the collection beam, respectively.

ReS_2, respectively. These results are consistent among more than 13 samples studied. Occasionally, mixed stacking order was observed in very thick samples, but the stacking order of thin samples can be determined by Raman without any ambiguity. The thicknesses of the two ReS_2 samples were measured with AFM (Figure S1) to be 56 nm (AB stacking) and 68 nm (AA stacking). The *b*-axis (Re−Re chain) can be determined with polarized Raman spectra of Mode V (Figure S2), which usually coincides with the cleaved edge.

Since ReS_2 is known to have multiple exciton levels that are anisotropic, we first conducted polarized photoluminescence (PL) measurements on both samples at different angles that are defined as the polarization of light against the *b*-axis. Both polarized Raman and PL measurements were conducted using an inVia confocal Raman microscope (Renishaw) with 532 nm excitation. A 2400 lines mm^{-1} grating was used in the Raman measurements. In order to control the polarization, the samples were mounted on a rotational stage. For PL, a 1200 lines mm^{-1} grating was used, and these results are presented in Figure 1b (AB stacking) and Figure 1e (AA stacking). Multiple peaks are identified in the PL spectra. The peak positioned around 1.4 eV is usually taken as the indirect band transition in multilayer ReS_2.[7] Alongside the indirect band transition, three exciton peaks are also identified. Figure 1c,f plots the PL peaks of all three excitons as a function of polarization angle. For both stacking orders, all three excitons' PL peak positions are relatively stable with varying polarization angles, which are obtained by fitting the PL spectra with the Voigt function (Figure S6). In AB stacking, the PL peaks are 1.48 eV for Exc. I, 1.52 eV for Exc. II, and 1.57 eV for Exc. III. In AA stacking, the PL peaks are 1.46 eV for Exc. I, 1.50 eV for Exc. II, and 1.56 eV for Exc. III. The PL positions of all three excitons in AB stacking are slightly higher than that of AA stacking. This is determined by the differences in both exciton binding energy and the bandgap in two stacking orders. In order to verify the Exc. III exists in both stacking AA and AB at room temperature, wavelength-resolved pump−probe experiment was performed around Exc. III level. A resonant feature shows in both stacking AA and stacking AB.

Optical transitions in multiplayer ReS_2 have been studied extensively.[6,7,15,16] Most results agreed that Exc. I and Exc. II polarize along different crystal orientations, for example, Exc. I mainly polarizes along 15° from the *b*-axis, and Exc. II along 90° (perpendicular) from the *b*-axis.[7] The PL spectra in Figure 1b,e are consistent with previous studies.[7] Ho et al. suggested that both Exc. I and Exc. II come from the transition of nonbonding Re 5d t_{2g} to nonbonding Re 5d t_{2g}*,[17] while Exc. III originates from nonbonding Re 5d t_{2g} to sulfur 3p states.[17,18] The energy level of excited states for Exc. I and Exc. II are very close, and both of these are close to the energy level of Exc. III. As a result, Exc. III can be treated as an excited state superposed by the excited states of both Exc. I and Exc. II.[16] From our simulation of the optical absorption spectrum (Figure 4b,e), finite values of the optical absorption from both directions (0° and 90°) are found around Exc. III level, which suggests the formation of Exc. III comes from a combined effect of Exc. I and Exc. II. As shown in Figure 1b,e, the photoluminescence of Exc. III (∼1.57 eV) in AA stacking is much more obvious than AB stacking, which is consistent with the aforementioned study.[12] To better resolve the Exc. III feature for different stacking orders, we measured the absorption of Exc. III for both samples as a function of irradiance with our home-built I-scan spectrometer at different polarization angles, with the laser photon energy resonating with Exc. III. A schematic diagram of the setup for the I-scan spectrometer is in Figure S5. The principle of the I-scan spectrometer is similar to a Z-scan spectrometer. The main difference is that the laser intensity of the I-scan is controlled

https://dx.doi.org/10.1021/acsphotonics.0c01225
ACS Photonics 2021, 8, 405−411

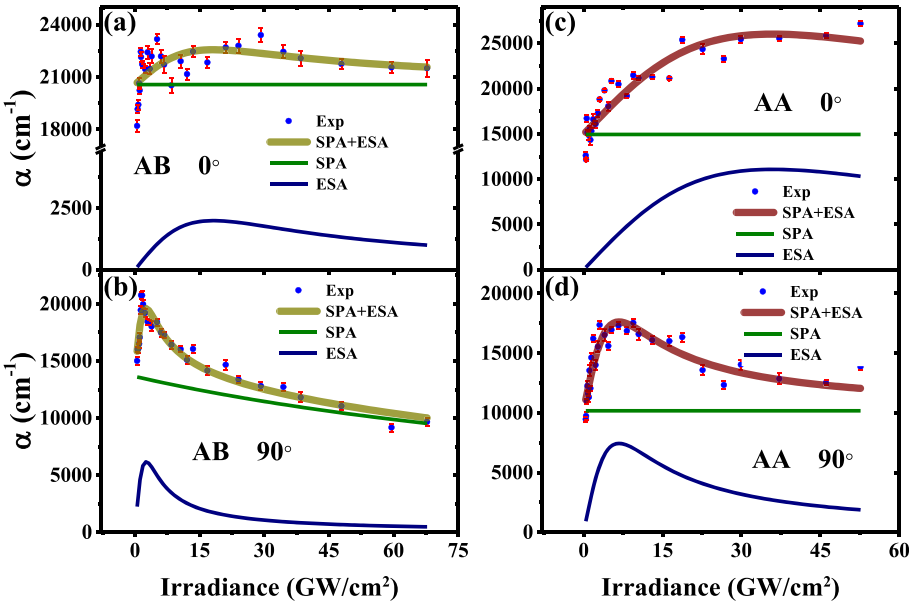

Figure 2. Absorption coefficient as a function of irradiance at 790 nm. (a, b) Results for AB stacking at 0° and 90°, respectively. (c, d) Results for AA stacking at 0° and 90°, respectively. The green lines represent the contribution from the SPA. The dark blue lines represent the contribution from the ESA. Error bars are obtained by adjusting the fitting range.

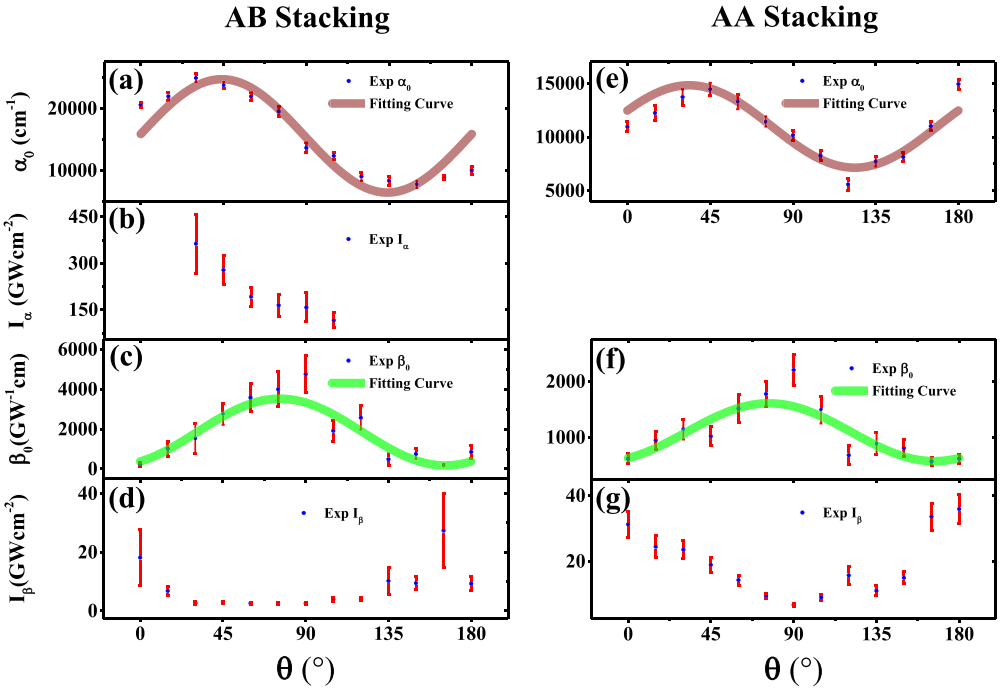

Figure 3. Nonlinear absorption parameters as a function of polarizations. (a–d) Results for AB stacking. (e–g) Results for AA stacking. The collected data sets are fitted by $\cos^2(\theta - \theta_{max}) + \varphi$ for α_0 and β_0 as solid lines.

by a neutral optical density filter instead of moving the sample across the laser focus point (Z-scan). I-scan is especially suitable for 2D materials prepared via mechanical exfoliation with limited surface areas. For the Z-scan measurement, a common assumption is that the reflectance of the sample stays constant and the absorption change is proportional to the transmittance change. To relax this assumption, we collected both the reflectance and the transmittance simultaneously in our I-scan spectrometer, and the complex refractive indices were derived from the transfer matrix method.[13] The absorption coefficient is related to the imaginary part of the complex refractive index.[13] The laser pulse used in the I-scan experiment has a 790 nm central wavelength (1.569 eV) with a 10 nm spectral width (fwhm). Under this condition, the laser photon energy resonates with Exc. III, and the spectral width is narrow enough to eliminate the broadening effect from Exc. II.[12] Comparing with PL, using I-scan to study nonlinear behavior of Exc. III resonantly can provide more accurate information because the PL spectra consist of the convoluted signal of multiple excitons and depend on both the oscillator strength and lifetime associated with each exciton.[19] Figure 2 shows the absorption coefficients (α) of AA and AB stackings

https://dx.doi.org/10.1021/acsphotonics.0c01225
ACS Photonics 2021, 8, 405–411

at 0° and 90° polarizations as a function of irradiance. For both stacking orders, regardless of polarization, α first increases with irradiance and then decreases. For AB_0°, AA_0°, and AA_90°, the values of α at higher irradiance are always larger than those at the lowest irradiance, which is usually called reversible saturable absorption (RSA). For AB_90°, when irradiance is above 14 GW/cm^2, the values of α decrease to be even smaller than that of the lowest irradiance. This phenomenon is called SA.

RSA may originate from free carrier absorption (FCA), two-photon absorption (TPA), or ESA. In ReS_2, ESA was proposed to be the most probable mechanism.[12,13] To observe ESA experimentally, the absorption of photons by the excited carriers to transit to higher energy levels has to be greater than that by the carriers on ground states. This requires a large number of excited carriers being initially excited to the excited states (photon energy resonant with excited state energy) and the laser pulse width (~400 fs) to be much shorter than the excited carrier lifetime. Both conditions are satisfied for Exc. III under our experimental conditions. A model that considers both SA and ESA was used to fit the experimental data:

$$\alpha = \frac{\alpha_0}{1 + \left(\frac{I}{I_\alpha}\right)} + \frac{\beta_0 I}{1 + \left(\frac{I}{I_\beta}\right)^2} \quad (1)$$

where α_0 is the SPA coefficient, I_α is the saturation irradiance associated with SPA, β_0 is the ESA coefficient, I_β is the saturation irradiance associated with the ESA, and I is the laser irradiance.

In Figure 2, both the overall fitting with eq 1 and the contributions from individual terms (SPA and ESA) are plotted. The solid green lines represent the contributions from SPA. For the cases of AB_0° (Figure 2a), AA_0° (Figure 2c), and AA_90° (Figure 2d), the SPA contributions show no dependence on irradiance.

This means the first term of eq 1 is a constant value, which indicates that the saturation irradiances (I_α) for these cases are extremely large. For AA stacking, the first term of eq 1 will be simply replaced with a constant value α_0. However, SA associated with SPA is prominent for AB_90°, which suggests that the SA effect in AB stacking has a very strong dependence on polarization. ESA, plotted as solid blue lines, is prominent in all cases and dominates for AB_0° (Figure 2a), AA_0° (Figure 2c), and AA_90° (Figure 2d). For the experimental data, at certain irradiances all cases show a clear turning point of absorption from increasing to decreasing. This phenomenon is only associated with ESA. The irradiance at which the turning point occurs relates to the ESA saturation irradiance, I_β. By comparing all the cases, it can be concluded that the I_β in stacking AB is smaller than that in stacking AA. For both stackings, the I_β at 90° polarization is smaller than that at 0°. Figure 3 shows the fitted parameters for both AB and AA stacking when rotating the laser polarization from 0° to 180° against the *b*-axis. The values of α_0 and β_0 in AB stacking are larger than those in AA stacking at all polarization angles. I_α only has meaningful values in AB stacking from 30° to 105° and disappears (extremely large fitted value and large standard deviation) for all angles in AA stacking. The values of I_β in AA stacking are larger than that of AB stacking. α_0 and β_0, the coefficients of SPA and ESA, are associated with the transition from ground state to Exc. III and from Exc. III to higher energy level, respectively. I_α and I_β, the saturation irradiance for SPA and ESA, are affected by both the transition probabilities and available states of Exc. III and the higher energy level. Due to the one-unit cell shift along the *a*-axis in AB stacking, the interlayer distance is decreased from 2.61 Å (interlayer distance of AA stacking) to 2.54 Å for the bulk from our simulation. The absorption coefficient measures the attenuation of the light irradiance per unit thickness. With a smaller interlayer distance in AB stacking, the light will pass through more layers per unit thickness, resulting in a larger absorption coefficient. Finite values of I_α in AB stacking for certain angles (30−105°) indicate that the maximum achievable states of Exc. III along these polarizations is much more limited compared with AA stacking.

In both AA and AB stackings, the angle-dependent α_0 and β_0 can be fitted with a function: $\xi \cos^2(\theta - \theta_{max}) + \eta$, with fitting parameters summarized in Table 1. This equation is related to the strength of transition at different angles. A larger amplitude of ξ means a greater change of absorption coefficient with θ. The base absorption coefficient is denoted as η. Lastly, θ_{max} is the particular angle at which the maximum absorption occurs. For both SPA (α_0) and ESA (β_0), ξ values in AB stacking are much larger than those in AA stacking, indicating that both transitions are more anisotropic in AB stacking. For both α_0 and β_0, the θ_{max} values stand between 15° and 90°, confirming that Exc. III is a superposition of Exc. I and Exc. II. The θ_{max} values for β_0 in AA and AB stackings are very similar and close to 90°. The θ_{max} values for α_0 in both stacking orders are closer to 15°, indicating a larger portion of the contribution from Exc. I. θ_{max} in AB stacking shifts by 10° to a larger value compared with AA stacking.

Table 1. Fitted Parameters with $\xi \cos^2(\theta - \theta_{max}) + \varphi$

	ξ		θ_{max}	
	AB	AA	AB	AA
α_0	18285 ± 2665	7683 ± 1120	44.1 ± 3.8°	33.6 ± 3.4°
β_0	3350 ± 408	1037 ± 169	75.9 ± 3.2°	76.6 ± 5.1°

From Figure 3b, the saturation irradiance (I_α) was only observed in AB stacking, with specific polarization angles ranging from 30° to 105°. This behavior could not be fully explained within the picture of ESA and the contribution from other physical mechanisms has to be considered, such as angle-dependent exciton−exciton annihilation (EEA). With a relatively large exciton density, the interaction between excitons cannot be neglected; the electron−hole pair of one exciton could recombine and transfer its energy to another adjacent exciton. The latter exciton would be excited further to a higher energy level. The EEA process is very similar to the Auger process of free charge carriers.[20]

The strength of EEA is closely related to the exciton spatial distribution and the polarization. Tran et al. did first-principles GW-BSE simulations to study the optical spectra of few-layer and bulk black phosphorus.[21] They found that the optical properties of excitons have a close relationship with their spatial anisotropy, which are optically bright only for the incident light polarized along the extended direction of their wave function.[21] Moreover, Wang et al. performed experiments to study the anisotropic excitons in monolayer black phosphorus[22] and observed that the PL of the exciton shows maximum intensity along the extended direction of the square of the ground-state exciton's electron wave function.[22] The photon's interaction with the material can be approximated by

https://dx.doi.org/10.1021/acsphotonics.0c01225
ACS Photonics 2021, 8, 405−411

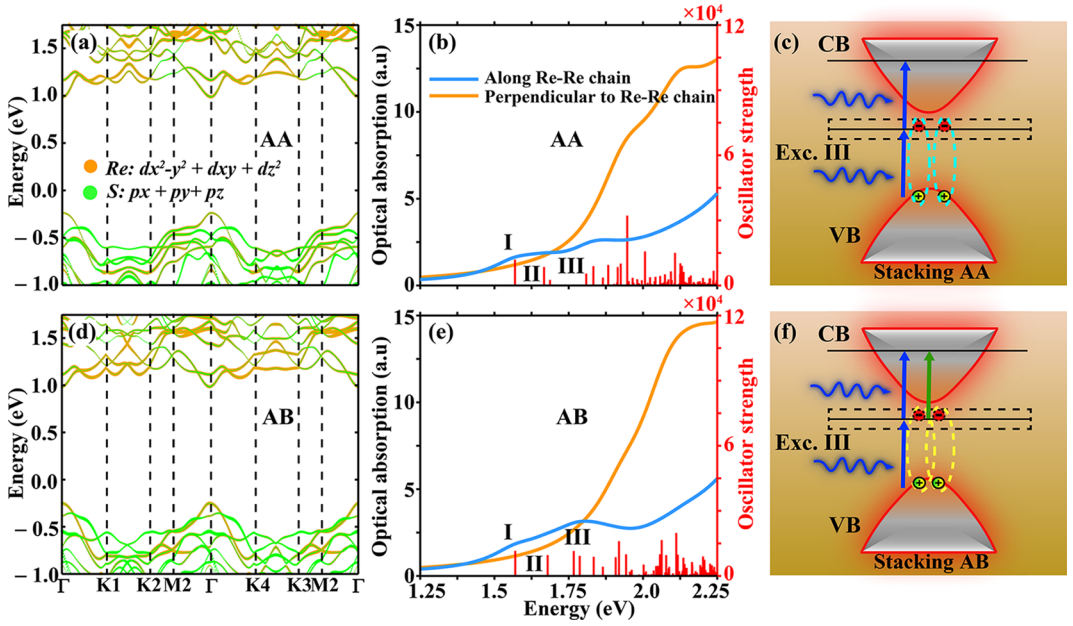

Figure 4. Band structures and optical transitions for different stacking orders in bulk ReS_2. (a, d) Orbital resolved band structures (Re 5d t_{2g} and sulfur 3p) for stacking AA and stacking AB, respectively. (b, e) Optical absorption spectra by G_0W_0−BSE along the Re−Re chain and perpendicular to the Re−Re chain direction for AA and stacking AB, respectively. The vertical red lines in the absorption spectra indicate the oscillator strength of the optical transitions, where I, II, and III represent the Exc. I, Exc. II, and Exc. III, respectively. (c, f) Schematic diagrams of the nonlinear absorption processes for stacking AA and stacking AB, respectively.

the transition dipole moment $\mu_{fi} = \langle f|\hat{\mu}\cdot\hat{\varepsilon}|i\rangle$, where $\hat{\mu} = \sum_j q\hat{r}_j$ is the dipole moment, $\hat{\varepsilon}$ is the unit vector of the light polarization, and i and f represent the initial and final state, respectively.[23] If the excitonic wave function is extended along a specific direction, the transition is preferable when the laser is polarized along the same direction, and the absorption coefficient should be larger.[7,24] The saturation of the Exc. III state in AB stacking observed in Figure 3b could originate from EEA. EEA determines the maximum exciton density that can be achieved at one state and was observed in many low dimensional systems, like graphene nanoribbons,[25] MoS_2 monolayer,[20] $MoSe_2$ monolayer,[26] and WSe_2 monolayer.[27] Shahnazaryan et al. studied the exciton−exciton interaction in transition metal dichalcogenide (TMD).[28] They found that the exciton exchange interaction energy results from the competition between the interexciton interaction enhancement and an intracarrier interaction decrease when increasing the screening length.[28] In other words, the exciton exchange interaction energy is affected by how the wave function spreads out so that different excitons can overlap with each other as well as how strong the intracarrier interaction is. Especially, the interaction of the excited exciton state (e.g., Exc. III of ReS_2) shows a clear increasing trend for a higher dielectric constant, while the ground state exciton (e.g., Exc. I and Exc. II) interaction strength does not change much.[28] On the other hand, the exciton size would increase with larger screening (higher dielectric constant),[29] which could effectively increase the overlapping probability for different excitons.[25] For a few-layer ReS_2, Sim et al. observed the signature of the exciton−exciton annihilation of the lowest exciton state with ultrafast pump−probe spectroscopy, which shows a much weaker layer dependence compared with other 2D TMDs.[30]

In Figure 4c,f, schematic diagrams of the absorption processes for different stacking orders are shown. For stacking AB, apart from the two blue arrows, which represent the SPA and ESA, a green arrow is added to represent the EEA process. The reason why the EEA process is significant in AB stacking could be understood from several aspects. First, in our previous paper,[12] the calculated dielectric constant in stacking AB is larger, which can induce a stronger screening effect and thus cause a stronger EEA.[28] Also, as shown in Figure 4b,e, the calculated oscillator strength in AB stacking around Exc. III level is actually stronger than that of stacking AA. A more extensive intracarrier interaction (oscillator strength) could lead to a stronger EEA. Second, comparing Figure 3a,e, the SPA coefficient (α_0) is larger in stacking AB, which indicates more excitons created with the same incident irradiance. As discussed above, one of the reasons could be a smaller interlayer distance in stacking AB. With more excitons in the real space, the probability of overlapping with one another would increase. Third, previous studies suggested that Exc. III corresponds to the optical transition from the nonbonding Re 5d t_{2g} to sulfur 3p states.[17,18] To get more insight, orbital-resolved band structures for different stacking orders are calculated with first-principles simulation and shown in Figure 4a,d. The orange color represents the Re 5d t_{2g} orbital, and the green color represents the sulfur 3p orbital. Comparing Figure 4a,d, for the valence band near the Γ point, the orbital contribution from the Re 5d t_{2g} orbital for stacking AB is about 0.488, much larger than that of stacking AA (0.335). For the conduction band, the orbital contribution from the sulfur 3p orbital is 0.225 in stacking AB, slightly larger than that in stacking AA (0.211). The results are summarized in Table S1. These values indicate that the possibility of optical transition to generate Exc. III is much higher in AB stacking, which leads to higher density of excitons and hence larger probability of exciton overlapping. The three aspects discussion above all suggest that EEA process is much more significant in AB stacking than in AA stacking. We want to mention that the orbital resolved band structures were done in the PBE level

https://dx.doi.org/10.1021/acsphotonics.0c01225
ACS Photonics 2021, 8, 405−411

without considering the many-body effects, which shows a direct bandgap for both stacking orders. GW calculation (considering the many-body effects) showed an indirect bandgap for bulk ReS_2.[31] However, the discussion above should still hold, since the difference between the direct bandgap and indirect bandgap is small.[7,31]

On the other hand, the angle-dependent transition probability for the ESA needs to be taken into account. From the fitted parameter θ_{max} of β_0 in Table 1, the transition is strongest around 76° for both stacking orders. The EEA process would be strong when both overlapping of exciton wave functions and transition strength are large. So, it is reasonable that I_α was only observed from 30° to 105° in AB stacking. Above 105°, β_0 keeps decreasing. Also, the decreased α_0 from 105° to 135° for AB stacking indicates a decreasing exciton size (deviating from the exciton's polarization) and a decreased number of excitons. All of these effects would make the EEA disappear due to decreased exciton overlapping probability and decreased transition strength. While for stacking AA, since both the α_0 and β_0 are much smaller, the EEA process might be weak in the range of irradiance investigated so that the saturation does not show.

The saturation of the higher energy level (I_β) can be understood as the Pauli blocking effect. Comparing the I_β between the stacking AB and stacking AA, the I_β in AB stacking shows a much smaller and nearly constant value from 30° to 120°, around a similar angle range at which the SPA in AB stacking shows saturation (finite values of I_β). This correlated behavior can be understood as an additional absorption channel (EEA) on top of ESA, which saturates the higher energy level at a much smaller irradiance. Power-dependent pump−probe experiments would be needed to gain a deeper understanding.

In summary, we studied the effect of stacking order on the nonlinear optical properties of ReS_2 with I-scan spectroscopy. We found that the saturation of the single-photon absorption (SPA) from the ground state (valence band) to Exc. III is only important in AB stacking at certain polarization angles, while excited-state absorption (ESA) from Exc. III to a higher energy level is prominent in both AA and AB stacking along all angles. Overall, both SPA and ESA are more anisotropic in AB stacking. ESA's saturation irradiance, I_β, is smaller in AB stacking than in AA stacking, which could be due to an additional absorption channel of exciton−exciton annihilation (EEA) in stacking AB. In the range of the irradiance investigated, the AB stacking ReS_2 could be used as a saturable absorber at a polarization angle from 30° to 105°. AA stacked ReS_2 could find applications in upper conversion lasers due to the saturable absorption being negligible at all angles. Our study reveals the profound impacts of stacking order on nonlinear optical properties in ReS_2.

■ ASSOCIATED CONTENT

Supporting Information

The Supporting Information is available free of charge at https://pubs.acs.org/doi/10.1021/acsphotonics.0c01225.

(1) Optical image and AFM. (2) Polarized Raman. (3, 4) Irradiance dependent absorption coefficient measured from 0° to 180° for AB and AA stacking, respectively. (5) schematic setup of I-scan spectrometer. (6) Representative fitting results for polarized PL (0°). (7, 8) Irradiance-dependent transmittance and reflectance for AB and AA stacking, respectively. (9) A schematic of the sample geometry. (10) Orbital-resolved band structures (Re 5d t_{2g} and Re 5d e_g) of the bulk ReS_2 (PDF)

■ AUTHOR INFORMATION

Corresponding Author

Yaguo Wang − *Department of Mechanical Engineering, The University of Texas at Austin, Austin, Texas 78712, United States; Texas Materials Institute, The University of Texas at Austin, Austin, Texas 78712, United States;* orcid.org/0000-0002-0448-5645; Email: yaguo.wang@austin.utexas.edu

Authors

Yongjian Zhou − *Department of Mechanical Engineering, The University of Texas at Austin, Austin, Texas 78712, United States*

Nikhilesh Maity − *Materials Research Centre, Indian Institute of Science, Bangalore 560012, India*

Jung-Fu Lin − *Department of Geological Sciences, Jackson School of Geosciences, The University of Texas at Austin, Austin, Texas 78712, United States; Texas Materials Institute, The University of Texas at Austin, Austin, Texas 78712, United States*

Abhishek K. Singh − *Materials Research Centre, Indian Institute of Science, Bangalore 560012, India;* orcid.org/0000-0002-7631-6744

Complete contact information is available at: https://pubs.acs.org/10.1021/acsphotonics.0c01225

Notes

The authors declare no competing financial interest.

■ ACKNOWLEDGMENTS

We thank Raul Montano for valuable suggestions. The authors are grateful for the support from the National Science Foundation (NASCENT, Grant No. EEC-1160494; CAREER, Grant Nos. CBET-1351881, CBET-1707080, Center for Dynamics and Control of Materials DMR-1720595); A.K.S. and N.M. thank the Materials Research Centre and Supercomputer Education and Research Centre of Indian Institute of Science for providing computing facilities.

■ REFERENCES

(1) Cao, Y.; Fatemi, V.; Fang, S.; Watanabe, K.; Taniguchi, T.; Kaxiras, E.; Jarillo-Herrero, P. Unconventional superconductivity in magic-angle graphene superlattices. *Nature* **2018**, *556* (7699), 43−50.

(2) Tran, K.; Moody, G.; Wu, F.; Lu, X.; Choi, J.; Kim, K.; Rai, A.; Sanchez, D. A.; Quan, J.; Singh, A.; Embley, J.; Zepeda, A.; Campbell, M.; Autry, T.; Taniguchi, T.; Watanabe, K.; Lu, N.; Banerjee, S. K.; Silverman, K. L.; Kim, S.; Tutuc, E.; Yang, L.; MacDonald, A. H.; Li, X. Evidence for moiré excitons in van der Waals heterostructures. *Nature* **2019**, *567* (7746), 71−75.

(3) Seyler, K. L.; Rivera, P.; Yu, H.; Wilson, N. P.; Ray, E. L.; Mandrus, D. G.; Yan, J.; Yao, W.; Xu, X. Signatures of moiré-trapped valley excitons in MoSe2/WSe2 heterobilayers. *Nature* **2019**, *567* (7746), 66−70.

(4) Shan, Y.; Li, Y.; Huang, D.; Tong, Q.; Yao, W.; Liu, W.-T.; Wu, S. Stacking symmetry governed second harmonic generation in graphene trilayers. *Science Advances* **2018**, *4* (6), eaat0074.

(5) Shi, J.; Yu, P.; Liu, F.; He, P.; Wang, R.; Qin, L.; Zhou, J.; Li, X.; Zhou, J.; Sui, X.; Zhang, S.; Zhang, Y.; Zhang, Q.; Sum, T. C.; Qiu, X.; Liu, Z.; Liu, X. 3R MoS_2 with Broken Inversion Symmetry: A

Promising Ultrathin Nonlinear Optical Device. *Adv. Mater.* **2017**, *29* (30), 1701486.
(6) Ho, C. H.; Huang, Y. S.; Tiong, K. K. In-plane anisotropy of the optical and electrical properties of ReS2 and ReSe2 layered crystals. *J. Alloys Compd.* **2001**, *317*−*318*, 222−226.
(7) Aslan, O. B.; Chenet, D. A.; van der Zande, A. M.; Hone, J. C.; Heinz, T. F. Linearly Polarized Excitons in Single- and Few-Layer ReS2 Crystals. *ACS Photonics* **2016**, *3* (1), 96−101.
(8) Liu, F.; Zheng, S.; He, X.; Chaturvedi, A.; He, J.; Chow, W. L.; Mion, T. R.; Wang, X.; Zhou, J.; Fu, Q.; et al. Highly sensitive detection of polarized light using anisotropic 2D ReS_2. *Adv. Funct. Mater.* **2016**, *26* (8), 1169−1177.
(9) Jang, H.; Ryder, C. R.; Wood, J. D.; Hersam, M. C.; Cahill, D. G. 3D Anisotropic Thermal Conductivity of Exfoliated Rhenium Disulfide. *Adv. Mater.* **2017**, *29* (35), 1700650.
(10) Corbet, C. M.; McClellan, C.; Rai, A.; Sonde, S. S.; Tutuc, E.; Banerjee, S. K. Field Effect Transistors with Current Saturation and Voltage Gain in Ultrathin ReS2. *ACS Nano* **2015**, *9* (1), 363−370.
(11) Liu, E.; Fu, Y.; Wang, Y.; Feng, Y.; Liu, H.; Wan, X.; Zhou, W.; Wang, B.; Shao, L.; Ho, C.-H.; Huang, Y.-S.; Cao, Z.; Wang, L.; Li, A.; Zeng, J.; Song, F.; Wang, X.; Shi, Y.; Yuan, H.; Hwang, H. Y.; Cui, Y.; Miao, F.; Xing, D. Integrated digital inverters based on two-dimensional anisotropic ReS2 field-effect transistors. *Nat. Commun.* **2015**, *6*, 6991.
(12) Zhou, Y.; Maity, N.; Rai, A.; Juneja, R.; Meng, X.; Roy, A.; Zhang, Y.; Xu, X.; Lin, J.-F.; Banerjee, S. K.; Singh, A. K.; Wang, Y. Stacking-Order-Driven Optical Properties and Carrier Dynamics in ReS2. *Adv. Mater.* **2020**, *32* (22), 1908311.
(13) Meng, X.; Zhou, Y.; Chen, K.; Roberts, R. H.; Wu, W.; Lin, J.-F.; Chen, R. T.; Xu, X.; Wang, Y. Anisotropic Saturable and Excited-State Absorption in Bulk ReS2. *Adv. Opt. Mater.* **2018**, *6* (14), 1800137.
(14) Qiao, X.-F.; Wu, J.-B.; Zhou, L.; Qiao, J.; Shi, W.; Chen, T.; Zhang, X.; Zhang, J.; Ji, W.; Tan, P.-H. Polytypism and unexpected strong interlayer coupling in two-dimensional layered ReS2. *Nanoscale* **2016**, *8* (15), 8324−8332.
(15) Wang, X.; Shinokita, K.; Lim, H. E.; Mohamed, N. B.; Miyauchi, Y.; Cuong, N. T.; Okada, S.; Matsuda, K. Direct and Indirect Exciton Dynamics in Few-Layered ReS2 Revealed by Photoluminescence and Pump-Probe Spectroscopy. *Adv. Funct. Mater.* **2019**, *29* (6), 1806169.
(16) Ho, C.-H.; Liu, Z.-Z. Complete-series excitonic dipole emissions in few layer ReS2 and ReSe2 observed by polarized photoluminescence spectroscopy. *Nano Energy* **2019**, *56*, 641−650.
(17) Ho, C. H.; Yen, P. C.; Huang, Y. S.; Tiong, K. K. Polarized electrolyte-electroreflectance study of ReS 2 and ReSe 2 layered semiconductors. *J. Phys.: Condens. Matter* **2001**, *13* (35), 8145.
(18) Ho, C. H.; Huang, C. E. Optical property of the near band-edge transitions in rhenium disulfide and diselenide. *J. Alloys Compd.* **2004**, *383* (1), 74−79.
(19) Jin, C.; Regan, E. C.; Wang, D.; Iqbal Bakti Utama, M.; Yang, C.-S.; Cain, J.; Qin, Y.; Shen, Y.; Zheng, Z.; Watanabe, K.; Taniguchi, T.; Tongay, S.; Zettl, A.; Wang, F. Identification of spin, valley and moiré quasi-angular momentum of interlayer excitons. *Nat. Phys.* **2019**, *15* (11), 1140−1144.
(20) Sun, D.; Rao, Y.; Reider, G. A.; Chen, G.; You, Y.; Brezin, L.; Harutyunyan, A. R.; Heinz, T. F. Observation of rapid exciton−exciton annihilation in monolayer molybdenum disulfide. *Nano Lett.* **2014**, *14* (10), 5625−5629.
(21) Tran, V.; Soklaski, R.; Liang, Y.; Yang, L. Layer-controlled band gap and anisotropic excitons in few-layer black phosphorus. *Phys. Rev. B: Condens. Matter Mater. Phys.* **2014**, *89* (23), 235319.
(22) Wang, X.; Jones, A. M.; Seyler, K. L.; Tran, V.; Jia, Y.; Zhao, H.; Wang, H.; Yang, L.; Xu, X.; Xia, F. Highly anisotropic and robust excitons in monolayer black phosphorus. *Nat. Nanotechnol.* **2015**, *10* (6), 517−521.
(23) Hanamura, E. Rapid radiative decay and enhanced optical nonlinearity of excitons in a quantum well. *Phys. Rev. B: Condens. Matter Mater. Phys.* **1988**, *38* (2), 1228.
(24) Ling, X.; Huang, S.; Hasdeo, E. H.; Liang, L.; Parkin, W. M.; Tatsumi, Y.; Nugraha, A. R.; Puretzky, A. A.; Das, P. M.; Sumpter, B. G.; et al. Anisotropic electron-photon and electron-phonon interactions in black phosphorus. *Nano Lett.* **2016**, *16* (4), 2260−2267.
(25) Murakami, Y.; Kono, J. Existence of an upper limit on the density of excitons in carbon nanotubes by diffusion-limited exciton-exciton annihilation: Experiment and theory. *Phys. Rev. B: Condens. Matter Mater. Phys.* **2009**, *80* (3), 035432.
(26) Kumar, N.; Cui, Q.; Ceballos, F.; He, D.; Wang, Y.; Zhao, H. Exciton-exciton annihilation in MoSe 2 monolayers. *Phys. Rev. B: Condens. Matter Mater. Phys.* **2014**, *89* (12), 125427.
(27) You, Y.; Zhang, X.-X.; Berkelbach, T. C.; Hybertsen, M. S.; Reichman, D. R.; Heinz, T. F. Observation of biexcitons in monolayer WSe 2. *Nat. Phys.* **2015**, *11* (6), 477−481.
(28) Shahnazaryan, V.; Iorsh, I.; Shelykh, I.; Kyriienko, O. Exciton-exciton interaction in transition-metal dichalcogenide monolayers. *Phys. Rev. B: Condens. Matter Mater. Phys.* **2017**, *96* (11), 115409.
(29) Perebeinos, V.; Tersoff, J.; Avouris, P. Scaling of Excitons in Carbon Nanotubes. *Phys. Rev. Lett.* **2004**, *92* (25), 257402.
(30) Sim, S.; Lee, D.; Lee, J.; Cha, M.; Cha, S.; Heo, W.; Cho, S.; Shim, W.; Lee, K.; Yoo, J.; et al. Role of weak interlayer coupling in ultrafast exciton-exciton annihilation in two-dimensional rhenium dichalcogenides. *Phys. Rev. B: Condens. Matter Mater. Phys.* **2020**, *101* (17), 174309.
(31) Gehlmann, M.; Aguilera, I.; Bihlmayer, G.; Nemšák, S.; Nagler, P.; Gospodarič, P.; Zamborlini, G.; Eschbach, M.; Feyer, V.; Kronast, F.; Młyńczak, E.; Korn, T.; Plucinski, L.; Schüller, C.; Blügel, S.; Schneider, C. M. Direct Observation of the Band Gap Transition in Atomically Thin ReS2. *Nano Lett.* **2017**, *17* (9), 5187−5192.

https://dx.doi.org/10.1021/acsphotonics.0c01225
ACS Photonics 2021, 8, 405−411